Springtime major pollution events by aerosol over Paris Area: From a case study to a multiannual analysis

Patrick Chazette, Philippe Royer

AGU PUBLICATIONS

JGR

Journal of Geophysical Research: Atmospheres

RESEARCH ARTICLE
10.1002/2017JD026713

Key Points:
- High coherence between ground-based and spaceborne (CALIOP) lidars for intense spring aerosol pollution events over the Paris Area
- Occurrence of the intense spring pollution events between 2007 and 2016 and their link with the aerosol optical properties
- Ground-based networks and spaceborne measurements, with multiple back trajectory analyses to characterize the intense spring pollutions

Correspondence to:
P. Chazette,
patrick.chazette@lsce.ipsl.fr

Citation:
Chazette P., and P. Royer (2017), Springtime major pollution events by aerosol over Paris Area: From a case study to a multiannual analysis, *J. Geophys. Res. Atmos.*, *122*, 8101–8119, doi:10.1002/2017JD026713.

Received 24 FEB 2017
Accepted 19 JUL 2017
Accepted article online 24 JUL 2017
Published online 3 AUG 2017

Springtime major pollution events by aerosol over Paris Area: From a case study to a multiannual analysis

Patrick Chazette[1] **and Philippe Royer**[2]

[1]Laboratoire des Sciences du Climat et de l'Environnement, Laboratoire mixte CEA-CNRS-UVSQ, UMR 8212, CEA Saclay, Gif-sur-Yvette, France, [2]LEOSPHERE, Paris, France

Abstract A study of the intense spring pollution events occurring between 2007 and 2016 on the Paris Area is presented using ground-based and spaceborne measurements. Emphasis is placed on 2011 where data included ground-based lidar measurements. This last period corresponds with the highest regional pollution levels of the past decade. The information threshold (daily average of (mass concentration of particles with aerodynamic diameter less than 10 μm) $PM_{10} > 50$ μg m^{-3}) was exceeded 16 times, while the alert threshold (daily average of $PM_{10} > 80$ μg m^{-3}) was exceeded twice. The information (alert) threshold exists to protect the most fragile people (the entire population). Ground-based and spaceborne measurements demonstrate the benefit of their synergy as each is representative of specific space and time scales. The operational products of the spaceborne instruments Cloud-Aerosol LIdar with Orthogonal Polarization (CALIOP) and the Moderate Resolution Imaging Spectroradiometer are used. For 2011, CALIOP vertical profiles are inversed to assess the backscatter to extinction ratio, which is then successfully compared with similar results derived from the CALIOP operational products, a ground-based lidar and Sun photometers. The aerosols are identified to be polluted continental and polluted dust aerosols following the criteria used for the inversion of the CALIOP profiles. Aerosol typing is consistent between the ground-based and spaceborne lidars, demonstrating the importance of CALIOP for other years where the ground-based lidar was not in operation. The main pollution sources responsible for the spring aerosol pollution, occurring during anticyclonic meteorological conditions, are identified as coming from Western Europe: Benelux, Rhine-Ruhr area, and the Lorraine area.

1. Introduction

Paris and its suburbs, with their ~12 million inhabitants, represent one of the three European megalopolises and the second by surface area. The Paris air mass is often found exceeding the health thresholds in $PM_{2.5}$ and PM_{10} (mass concentration of particles with aerodynamic diameter less than 2.5 and 10 μm, respectively). This requires measures to regulate vehicular traffic, which is one of the main sources of aerosol or aerosol precursor emissions around the French capital (for ~15–20%). In background locations, an exceeding of the threshold is mainly related to anticyclonic conditions, which favor the stagnation or recirculation of pollutants. In this article, we will describe a severe air pollution event caused by such particles during springtime. For that purpose, we will use ground-based lidar observations and characterize what has been the occurrence of similar environmental conditions mainly between 2007 and 2016.

Studying and reporting aerosol pollution events is a public health necessity. Indeed, several epidemiological studies have established the link between the concentration of fine particles and pulmonary disorders [*Chauhan and Johnston*, 2003], cardiovascular diseases [*Brook et al.*, 2004], and lung cancers [*Pope et al.*, 2002]. A study performed in the United States between 1970 and 2000 showed that a decrease of 10 μg m^{-3} of $PM_{2.5}$ concentrations would increase life expectancy between 5 and 9 months [*Pope et al.*, 2009]. According to the Clean Air for Europe program [*Amann et al.*, 2005], fine particles were responsible for 386,000 premature deaths and 110,000 serious hospitalizations in the European Union (EU 25 countries) for the year 2000. The same study established a mean reduction of life expectancy by 9 months and by up to 36 months in areas exposed to higher levels of pollution (Benelux, Po Valley, and Paris Agglomeration).

To mitigate the impact of air pollution on populations, the EU is trying to reduce PM_{10} and $PM_{2.5}$. Since 2005, European regulation imposes an annual mean of standard PM_{10} concentration lower than 40 μg m^{-3}, and a daily mean of 50 μg m^{-3} not to be exceeded more than 35 times per year (directive 2008/50/EC of 21 May 2008, http://eur-lex.europa.eu/LexUriServ/ LexUriServ.do?uri = OJ:L:2008:152:0001:0044:en:PDF).

World Health Organization (WHO) air quality guidelines are much more environmentally conscious, with an annual threshold mean of 20 $\mu g\ m^{-3}$ and a daily threshold mean of 50 $\mu g\ m^{-3}$ not to be exceeded more than 3 times per year (http://www.euro.who.int/__data/assets/pdf_file/0005/78638/E90038.pdf?ua=1). Regarding $PM_{2.5}$, the reduction of such concentrations is meant to be gradual, with annual threshold mean target values of 25 $\mu g\ m^{-3}$ in 2015 and 20 $\mu g\ m^{-3}$ in 2020. Reaching these target values would enable an increase of 3 months of life expectancy and avoid 135,000 deaths and 47,000 hospitalizations compared to the year 2000. WHO recommendations for $PM_{2.5}$ are 10 $\mu g\ m^{-3}$ in annual mean.

The Paris Area is one of the hot spots for air pollution in Western Europe, along with the Po Valley [*Highwood et al*., 2007; *Finardi et al*., 2014; *Beekmann et al*., 2015], the London megapolis [*McMeeking et al*., 2012], and the BeNeLux/Rhine-Ruhr area [*Gladtke*, 1998]. Several experimental campaigns and theoretical studies have been performed to study the air quality in the Paris Area, under the framework of various international projects: in summer 1998–2000 during the "Air Pollution Over the Paris Region" (ESQUIF) [e.g., *Vautard et al*., 2003; *Chazette et al*., 2005; *Tombette et al*., 2008], in summer 2007 during the "Lidar pour la Surveillance de l'AIR" campaign [*Raut and Chazette*, 2009], and more recently in summer and winter 2009 with the "megacities: emissions, urban, regional and global atmospheric pollution and climate effects, and integrated tools for assessment and mitigation program" [e.g., *Royer et al*., 2011b; *Freutel et al*., 2013; *Pikridas et al*., 2015]. To our knowledge, few detailed scientific studies have been performed during spring.

This study is a continuation of these previous studies on aerosols influencing the air quality over the Paris megalopolis. It relies more heavily on aerosol measurements within the atmospheric column thanks to lidar technology. Many chemical analyses were performed close to the surface to characterize the pollution aerosol [e.g., *Pikridas et al*., 2015], but the chemical components evolve within the planetary boundary layer and the lower free troposphere. The relevant approach is to use airborne measurements; however, that is only feasible during specific field campaigns [e.g., *McMeeking et al*., 2012]. Moreover, the aerosol sampling has significant uncertainties during airborne measurements [e.g., *Johnson et al*., 2008]. Chemical transport models, on the other hand, are often used, yet remain limited in their capability for major pollution events [e.g., *Royer et al*., 2011b]. This is mainly because they are difficult to validate over long periods of time within the tropospheric column. Moreover, the models diverge from one another depending on the situation encountered. Hence, we present a complementary remote sensing means of investigation to characterize the aerosol pollution events and to assess the main aerosol typing on a decadal scale.

The synergy with spaceborne instruments (e.g., the Moderate Resolution Imaging Spectroradiometer (MODIS) and the Cloud-Aerosol LIdar with Orthogonal Polarization (CALIOP)), and the ground-based measurements of the Paris air quality network (AIRPARIF) (http://www.airparif.asso.fr/) and aerosol robotic network (AERONET) (http://aeronet.gsfc.nasa.gov/), as well as the coupling to back trajectory modeling, make it possible to significantly enrich lidar observation and help identify the mechanics of pollution. We focus on extreme pollution events occurring over Western Europe in March–April, with a special interest in the pollution event of March 2011, which was sampled by ground-based lidar in the Paris Area. After presentation of the analysis tools in section 2, the case study of the high-pollution event occurring over Paris in March 2011 is analyzed in section 3 via ground-based in situ observations, vertical atmospheric structure, meteorological conditions, and satellite measurements. This first phase will provide confidence in the use of the spaceborne lidar CALIOP, which gives a more global view of the strongest events of spring aerosol pollution. Section 4 is dedicated to the longer-term analysis of the spring pollution events for the period 2007–2016.

2. Analysis Tools

2.1. Active Remote Sensing

2.1.1. Ground-Based Aerosol Lidar System: ALS 450

The ground-based lidar (GBL) system used in this study is the ALS450® lidar manufactured by Leosphere and initially developed by the Commissariat à l'Energie Atomique (CEA) and the Centre National de la Recherche Scientifique (CNRS) [*Royer et al*., 2011b]. It was located ~30 km south of Paris (48.708 N, 3.482 E) during March 2011. The main characteristics of this lidar are summarized in Table 1. It is based on an Ultra® Nd:YAG laser manufactured by Quantel, delivering 6 ns width pulses at the repetition rate of 20 Hz with a mean pulse energy of 16 mJ at a wavelength of 355 nm. This instrument operated on board the Mobile Atmospheric Station [e.g., *Raut and Chazette*, 2007] on the CEA-Saclay site, 30 km south of Paris. This system is

Table 1. Main Lidar Characteristics Used for the Case Study of March 2011

	ALS 450	CALIOP	WLS 70
Laser	Nd:YAG, flash-pumped, Q-switched Ultra (Quantel)	Nd:YAG, diode-pumped, Q-switched	Master Oscillator + Erbium Doped Fiber Amplifier
Pulse length	5 ns	20 ns	400 ns
Energy	16 mJ at 355 nm	110 mJ at 532 and 1064 nm	1543 nm
Frequency	20 Hz	20.16 Hz	
Reception channels	// 355 nm⊥ 355 nm	Total 1064 nm// 532 nm⊥ 532 nm	
Reception diameter	15 cm	100 cm	10 cm
Field-of-view	~ 4 mrad	130 mrad	
Full overlap	~ 200 m		100 m
Detector	Photomultiplier tubes	Photomultiplier tubes (532 nm)Avalanche photodiode (1064 nm)	
Filter bandwidth	0.3 nm	35 pm (532 nm)400 pm (1064 nm)	
Vertical resolution	0.75 m (analog)7.5 m (photon counting)	30 m between 0 to 8.2 km	50 m
Total size	Head: $65 \times 35 \times 18$ cm^3 Electronic: $70 \times 60 \times 60$ cm^3	$149 \times 184 \times 131$ cm^3	$80 \times 65 \times 55$ cm^3
Lidar head and electronic weight	$<$ 50 kg	283 kg	70 kg

particularly well adapted to air pollution and tropospheric aerosol study thanks to its full overlap reached at about 200 m and its high vertical resolution of 0.75 m (15 m after filtering). It is composed of a receiver channels dedicated to the measurement of the copolar and cross-polar signals at 355 nm. The detection is carried out by photomultiplier tubes and narrowband filters with a bandwidth of 0.3 nm. It gives access to the aerosol optical properties (depolarization ratio and extinction coefficient in synergy with Sun photometer measurements) and atmospheric structures (planetary boundary layer (PBL) and residual layer heights, aerosol and cloud layers) with a temporal resolution of 1 min. The inversion procedure to retrieve the aerosol optical properties is well discussed in several previous articles where uncertainty sources are exhaustively quantified [e.g., *Raut and Chazette*, 2009; *Royer et al*., 2011a; *Chazette et al*., 2012].

2.1.2. Wind Lidar System: WINDCUBE70

The WINDCUBE70 Doppler lidar is a commercial coherent Doppler wind lidar, developed and manufactured by Leosphere for meteorological and wind energy applications (Table 1). It is based on a pulsed Erbium-Doped Fiber Laser emitting at 1543 nm, an all fiber optical architecture and a coherent detection for Doppler analysis. The lidar measures and displays in real time the relative backscattering coefficient for each altitude, as well as the wind direction and horizontal and vertical wind components. Wind components are retrieved, with a vertical resolution of 50 m, thanks to four successive lines-of-sight along a cone, also known as Doppler Beam Swinging (DBS) method. The scattering target is the aerosol for this type of lidar. Therefore, it is limited in its range distance to a value close to the PBL height, typically between 100 and 2000 m. The lidar is embedded in a IP65 compact casing ($80 \times 65 \times 55$ cm^3) with storage and communication devices, allowing autonomous atmospheric surveys during long periods. The precision on the wind speed measurement is ~0.3 m s^{-1} for a speed range between 0 and 50 m s^{-1}. The wind lidar operated next to the ALS 450 lidar.

2.1.3. CALIOP Spaceborne Lidar

Cloud-Aerosol LIdar with Orthogonal Polarization (CALIOP) is a spaceborne nadir-pointing lidar launched on 28 April 2006 aboard Cloud-Aerosol Lidar and Infrared Pathfinder Satellite Observations (CALIPSO, http://www-calipso.larc.nasa.gov) to join the Afternoon Constellation (A-train) [e.g., *Stephens et al*., 2002]. Its 705 km high Sun-synchronous orbit has a cycle repetitivity of 16 days. The main characteristics of the CALIOP lidar are summarized in Table 1. The emission is based on a diode-pumped Nd:YAG producing linearly polarized pulses of light at 1064 and 532 nm with a mean pulse energy of 110 mJ and a repetition rate of 20.25 Hz (i.e., a horizontal resolution of 333 m [*Winker et al*., 2003]). The receiver is composed of a 1 m telescope and three detectors to measure the backscattered signal at 1064 nm and the parallel and perpendicular components of the 532 nm return. The high vertical resolution of CALIOP (30–60 m) provides information over land and sea on optical, physical, and structural properties of aerosols and clouds. Details on the CALIOP instrument, data acquisition, and science products are given by *Winker et al*. [2007].

For a comparison with the ground-based lidar in spring 2011, we have employed both the total and the perpendicular attenuated backscatter coefficient at 532 nm from CALIOP level-1 calibrated data product with a

horizontal resolution (~0.3 km). CALIOP lidar profiles at 532 nm are constrained using the coincident aerosol optical thickness (AOT) at 550 (AOT_{550}) measured by Aqua-MODIS radiometer along CALIOP track. A similar approach has already been developed for the study of dust aerosols [e.g., *Berthier et al*., 2006] and pollution aerosols over the Po Valley [*Royer et al*., 2010]. AOT_{550} used for the inversion is computed by weighting MODIS AOT pixels by the distance between pixel center and CALIOP profile in a radius of 20 km around CALIOP profile. An individual CALIOP level-1 profile is associated to a signal-to-noise ratio (SNR) in the PBL close to 1.5, which is not enough to retrieve the aerosol extinction profile. After cloud clearing, CALIOP mean profiles and coincident AOT_{550} are thus averaged over 45 individual profiles, which correspond to a horizontal resolution of ~15 km. The resulting SNR of the mean CALIOP profile ranges from 6 to 43 with a mean value of ~18 in the PBL after applying a low-pass filtering on the lidar data and reducing the lidar vertical resolution to ~100 m. The mean CALIOP profile is then inverted with a classical Klett algorithm [*Klett*, 1985], which requires a dichotomous approach on the lidar ratio (LR) [see *Royer et al*., 2010].

When available, the CALIOP level-2 data (version 4.10) are also used for the analyses of the strong aerosol pollution events. We mainly consider the aerosol typing, which was corrected in version 4.10, as noted in *Burton et al*. [2015]. Some CALIOP-derived vertical profiles of aerosol extinction coefficient at 532 nm are also used.

2.2. Passive Remote Sensing

2.2.1. MODIS Spaceborne Radiometers

Terra and Aqua Moderate Resolution Imaging Spectroradiometer (MODIS) [*Salomonson et al*., 1989; *King et al*., 1992] reached their heliosynchronous orbits on December 1999 and May 2002, respectively (http://modis.gsfc.nasa.gov). The polar orbit of Terra (http://terra.nasa.gov) passes over the equator from north to south in the morning, whereas Aqua (http://aqua.nasa.gov), within the A-train constellation, has an ascending node over the equator during the afternoon. The MODIS radiometers are composed of 36 spectral bands, or groups of wavelengths, from 400 nm to 1440 nm. Their wide swath of 110° (i.e., 2330 km) provides a global coverage of the Earth's surface over 1 to 2 days with a resolution between 250 and 1000 m at ground level depending on the band. Here we used the aerosol optical thickness at 550 nm (τ_{550}) from Aqua-MODIS aerosol level-2 data product. This product (http://modis.gsfc.nasa.gov) is given with a spatial resolution of 10×10 km^2 at nadir. τ_{550} is given with an uncertainty of $\pm 0.05 \pm 0.2\ \tau_{550}$ over land [*Chu et al*., 2002].

2.2.2. AERONET Sun Photometer Network

The AErosol RObotic NETwork (AERONET) is an automatic and global network of Sun photometers providing long-term and continuous monitoring of aerosol optical, microphysical, and radiative properties (http://aeronet.gsfc.nasa.gov/). Each site is composed of a Sun and sky scanning spectral radiometer manufactured by CIMEL. For direct solar measurement, eight spectral bands are generally used between 340 and 1020 nm. The five standard wavelengths are 440, 670, 870, 940, and 1020 nm. The aerosol optical thickness (AOT) data are computed for three data quality levels: level 1.0 (unscreened), level 1.5 (cloud-screened), and level 2.0 (cloud screened and quality assured). The total uncertainty on AOT is $<\pm 0.01$ for $\lambda > 440$ nm and $<\pm 0.02$ for $\lambda < 440$ nm [*Holben et al*., 1998]. Nevertheless, additional bias may exist when thin cirrus is present and not screened in the AERONET level-2 products [*Chew et al*., 2011]. To limit this, lidar profiles are used to identify or not the presence of cirrus. Indeed, thin cirrus is of large horizontal extension and may simultaneously affect the lidar and Sun photometer measurements. Here we used level 2 AOT data from Paris and Palaiseau stations at 340, 380, 440, and 500 nm.

2.3. AIRPARIF Network

AIRPARIF (http://www.airparif.asso.fr) is the regional operational network in charge of air quality survey over the Paris Area. It is composed of 68 stations spread out in a radius of 100 km within and around Paris measuring critical gases (CO, O_3, NO, NO_2, and SO_2) and/or aerosol concentrations (PM_{10} and $PM_{2.5}$) hourly. Two different types of stations are distinguished: 26 stations close to traffic sources and 42 background (urban, peri-urban, or rural) stations. From the entire set of measurements, here we consider PM_{10} and $PM_{2.5}$ concentrations measurements performed with automatic TEOM instruments (Tapered Element Oscillating Microbalance) [*Patashnick and Rupprecht*, 1991]. The uncertainty on PM_{10} concentrations measured with TEOM instrument has been assessed to be between 9 and 20% (AIRPARIF, http://www.airparif.asso.fr/telechargement/telechargement-statistique). TEOM measurements correspond to dry PM_{10} or $PM_{2.5}$, as sampling is performed through a warmed inlet at a temperature of ~50°C.

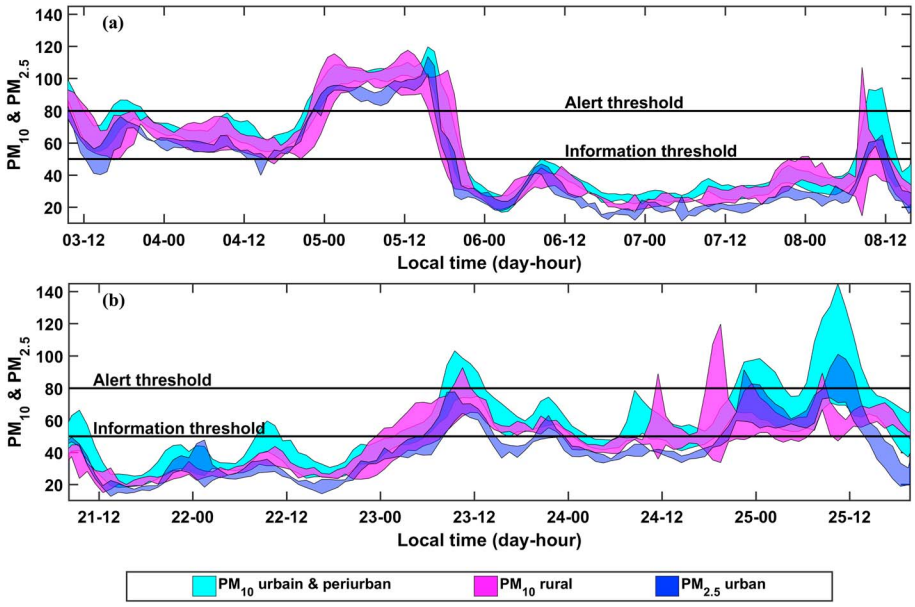

Figure 1. Temporal evolution of both PM_{10} and $PM_{2.5}$ observed by the ground-based AIRPARIF network between (a) 3 and 8 March 2011 and (b) 21 and 25 March 2011.

3. Pollution Events of March 2011: Two Case Studies

The two pollution events described here occurred over the Paris megalopolis between 3 and 9, and 21 and 25 March 2011. They were selected because they were sampled from the GBL. The identification of the pollution is made possible by both local air quality network and lidar profiling. The HYbrid Single-Particle Lagrangian Integrated Trajectory (HYSPLIT) model [*Draxler and Rolph*, 2015] is used to determine the air mass origins with a constraint on the aerosol plume altitudes derived from the GBL. The vertical structure of the atmosphere is analyzed by both the ground-based and spaceborne CALIOP lidars. The GBL is also a good tool to give us confidence in the CALIOP operational products for their widespread use over time and space. The spatial extent of the pollution events is covered by MODIS and CALIOP spaceborne measurements.

3.1. Air Quality Network Observations

Ground-based in situ measurements from AIRPARIF are used to identify the two pollution events on March 2011 corresponding with the available lidar data. Pollution events are distinguished when the daily PM_{10} concentration exceeds 50 $\mu g\ m^{-3}$, which corresponds to the information threshold as defined by the air quality criteria in the French Environment Code (articles R221-1 to R221-3). It also includes cases of very high pollution situations (daily mean concentration higher than 80 $\mu g\ m^{-3}$) based on the alert threshold. The information (alert) threshold corresponds with the concentration of pollutants in the atmosphere, to which short-term exposure presents a risk to the health of fragile populations (the entire population). The information threshold of 50 $\mu g\ m^{-3}$ is derived from the European directive 2008/50/EC of 21 May 2008 from the European Parliament, based on the recommendations of the World Health Organization.

The temporal evolution of PM_{10} for nontraffic stations is shown in Figure 1. The pollution events occurring during the two periods, between 3 and 8 March 2011, and 21 and 25 March 2011, are clearly visible from PM_{10} reaching concentrations higher than 100 $\mu g\ m^{-3}$. The low standard deviations of PM_{10} concentration observed are indicative of the pollution event affecting the entire Ile-de-France area and thus are not solely due to local emissions, whose effects are more heterogeneous on the space-scale of the Paris Area.

On 5 March 2011 (Figure 1a), 15 background stations exceeded the alert threshold. High PM_{10} concentrations were also observed during the previous 2 days, with 15 stations exceeding the information threshold (daily

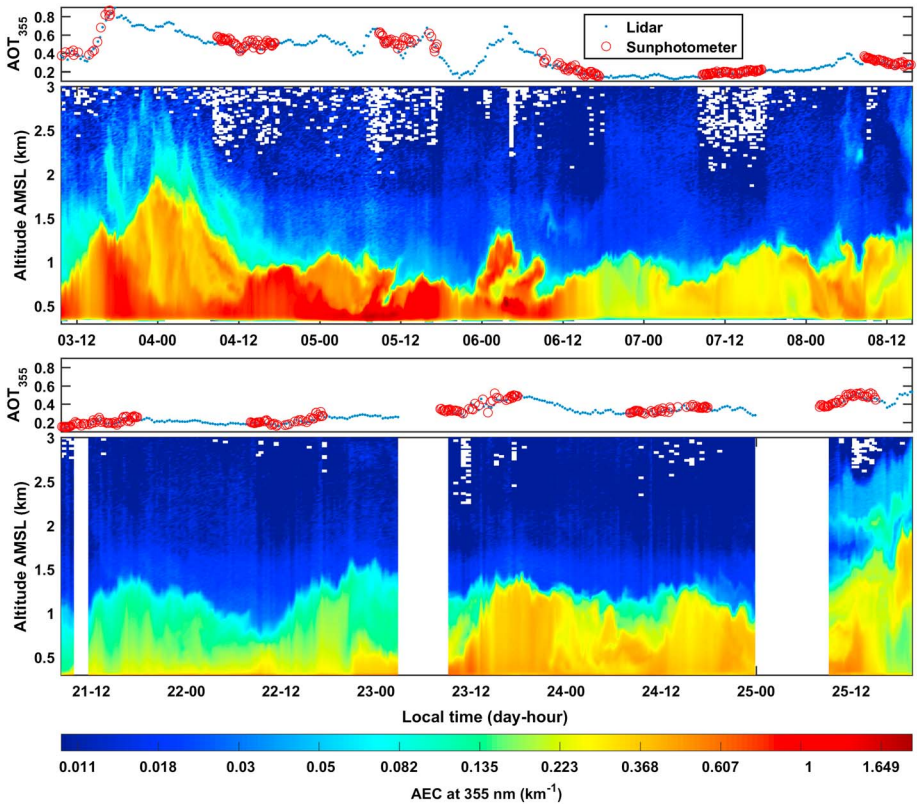

Figure 2. Sun photometer AOT used for the inversion and lidar-derived AOT at 355 nm (top panel). Time-height evolution of the lidar-derived aerosol extinction coefficient (AEC) at 355 nm observed above the Paris Area between (a) 3 and 9 March 2011 and (b) 21 and 25 March 2011. The top graph shows the temporal evolution of aerosol optical thickness (AOT) at 355 nm for both the Sun photometer and the lidar.

mean higher than 50 $\mu g\ m^{-3}$). The pollution event stopped abruptly on 6 March, with PM_{10} concentrations falling to 30 $\mu g\ m^{-3}$. A second pollution event began 23 March, with PM_{10} exceeding 50 $\mu g\ m^{-3}$ through 25 March (Figure 1b). Peaks exceeding 80 $\mu g\ m^{-3}$ occurred on both days.

3.2. Aerosols in the Atmospheric Column

3.2.1. Local Measurements

As shown in Figure 2, most of the aerosol load is trapped in the planetary boundary layer (PBL) and the nocturne layer (NL). The PBL top increases during the afternoon to reach between 1 and 1.4 km above the mean sea level (amsl), whereas the NL stays lower than ~0.4 km amsl. For the first pollution event (Figure 2a), the highest aerosol extinction coefficient (AEC) values (up to 0.5 km^{-1}) are observed between 3 and 5 March, with values exceeding 1.5 km^{-1} on 5 March when the PBL top is lower. On the night of 3 and 4 March, we note a significant contribution of a residual layer located between ~0.5 and 2 km amsl. On average, the PBL top is substantially higher during the second pollution event (Figure 2b), with an AEC of less than 0.6 km^{-1}.

The AOT derived from the Sun photometer and the lidar is also given at the top of Figures 2a and 2b. As in *Chazette et al.* [2016], the Sun photometer is used to constrain the inversion of lidar measurements and retrieve the equivalent backscatter to extinction coefficient (BER, product of the backscatter phase function and the single-scattering albedo) of the total aerosol column. We will hereafter use this parameter, as it is more directly representative of the aerosol properties than the lidar ratio. It is worth noting that the AOT is generally higher than 0.4 at 355 nm when pollution occurred. It exceeds 0.8 on 5 March. Such values are significantly higher than the mean AOT value over the Paris Area, which is close to 0.2 at the same wavelength for all the period between 24 July 1999 and 17 March 2016 (Figures 3a and 3c).

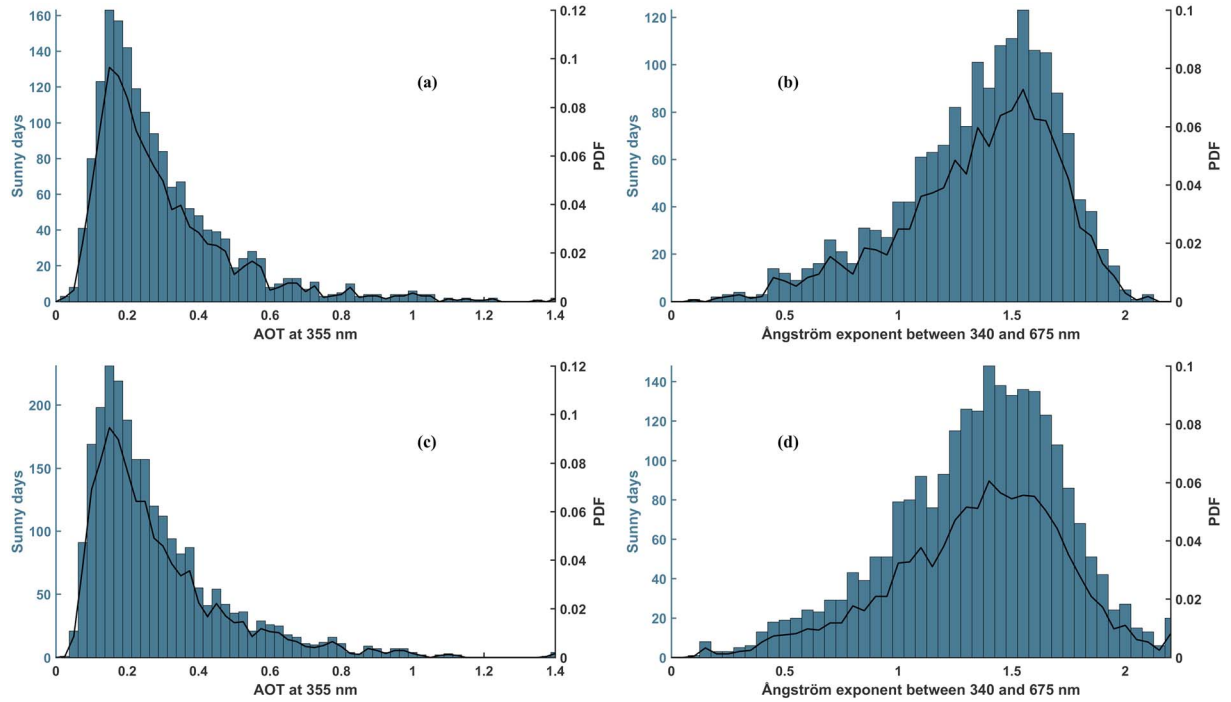

Figure 3. Daily aerosol optical thickness (AOT) at 355 nm between 24 July 1999 and 17 March 2016 derived from the Sun photometer of the AERONET sites of (a) Paris and (c) Palaiseau. The corresponding daily Ångström exponents are given in Figures 3b and 3d for Paris and Palaiseau, respectively. The probability density functions (PDF) are also given (right *y* axis).

For the two pollution episodes, the daily mean values of all representative variables are given in Table 2. We note that the particle depolarization ratio (PDR) retrieved from the GBL is significantly higher during the end of the second event, with values reaching 20% and representative of dust-like particles [e.g., *Chazette et al*., 2015]. The Sun photometer-derived visible Ångström exponent (AE) supports the same conclusion with a value close to 1, compared to the one of polluted aerosol generally

Table 2. Aerosol Optical Properties Derived From Ground-Based Sun Photometers and the Spaceborne Instruments MODIS and CALIOP During the Pollution Events on 3–8 and 21–25 March 2011[a]

	BER (sr^{-1})				PDR (%)		AOT	
			Sun Photometer 440 nm (*N*)			Sun Photometer		
March 2011	GBL Lidar 355 nm	CALIOP 532 nm	Paris	Palaiseau	GBL Lidar 355 nm	Ångström Exponent 440–675 nm	Sun Photometer 355 nm	MODIS 550 nm
3	0.015 ± 0.003	-	(8) 0.012 ± 0.003	(8) 0.013 ± 0.002	2–5	1.4 ± 0.05	0.6 ± 0.2	0.27 ± 0.02
4	0.012 ± 0.002	0.014 ± 0.005			1–7	1.6 ± 0.03	0.5 ± 0.04	0.26 ± 0.03
5	0.014 ± 0.005	0.016 ± 0.005			2–7	1.3 ± 0.06	0.53 ± 0.05	0.39 ± 0.04
6	0.021 ± 0.004	-	(7) 0.020 ± 0.001	(6) 0.021 ± 0.002	1–7	1.4 ± 0.1	0.22 ± 0.06	0.13 ± 0.02
7	0.014 ± 0.002	0.019 ± 0.009	(9) 0.019 ± 0.003	(11) 0.019 ± 0.002	1–5	1.7 ± 0.1	0.19 ± 0.02	0.10 ± 0.02
8	0.019 ± 0.003	-	(8) 0.017 ± 0.002	(11) 0.021 ± 0.003	3–8	1.2 ± 0.07	0.31 ± 0.03	0.21 ± 0.01
21	0.019 ± 0.003	-	(8) 0.020 ± 0.002	(11) 0.017 ± 0.002	4–7	1.8 ± 0.08	0.2 ± 0.004	-
22	0.022 ± 0.004	-	(8) 0.021 ± 0.003	(7) 0.019 ± 0.005	3–9	1.6 ± 0.1	0.22 ± 0.04	0.17 ± 0.02
23	0.026 ± 0.005	0.013 ± 0.005	(7) 0.016 ± 0.002	(8) 0.019 ± 0.002	4–10	1.4 ± 0.2	0.4 ± 0.07	0.29 ± 0.02
24	0.034 ± 0.004	-	(5) 0.018 ± 0.003	(9) 0.020 ± 0.002	5–12	1.2 ± 0.05	0.34 ± 0.03	0.27 ± 0.02
25	0.034 ± 0.003	0.018 ± 0.005	(7) 0.018 ± 0.004	(8) 0.026 ± 0.003	9–20	1.0 ± 0.1	0.45 ± 0.05	0.36 ± 0.02

[a]The backscatter to extinction ratio (BER) is derived from CALIOP data inverted using MODIS AOT as a constraint and the operation product version 4.10. The aerosol optical thickness (AOT) is given for each passive remote sensing instrument. The number of data *N* is also given for Sun photometer-derived BER. The gray area is when the Sun photometer data level 1.5 are used, as the single-scattering albedo is not available for level 2.

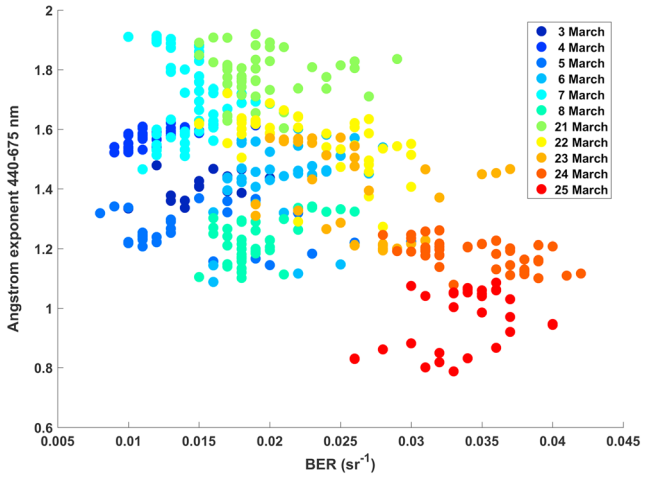

Figure 4. Scatterplot between the Ångström exponent and the lidar-derived backscatter to extinction ratio. For both pollution events, each day is identified by a specific color.

close to 1.5 as shown in Figures 3b and 3d [see also *Raut and Chazette*, 2007]. Moreover, the scatterplot of the AE against the BER (Figure 4) significantly isolates the contribution of 24–25 March. For the other days, the nature of the aerosols seems very similar. Considering again Table 2, for both AERONET stations of Paris and Palaiseau, the Sun photometer-derived BER matches the one retrieved from the lidar at the beginning of March, even if the wavelengths are different. For the second part of March 2011, high cloud presence and/or the level of AOT make it difficult to assess the

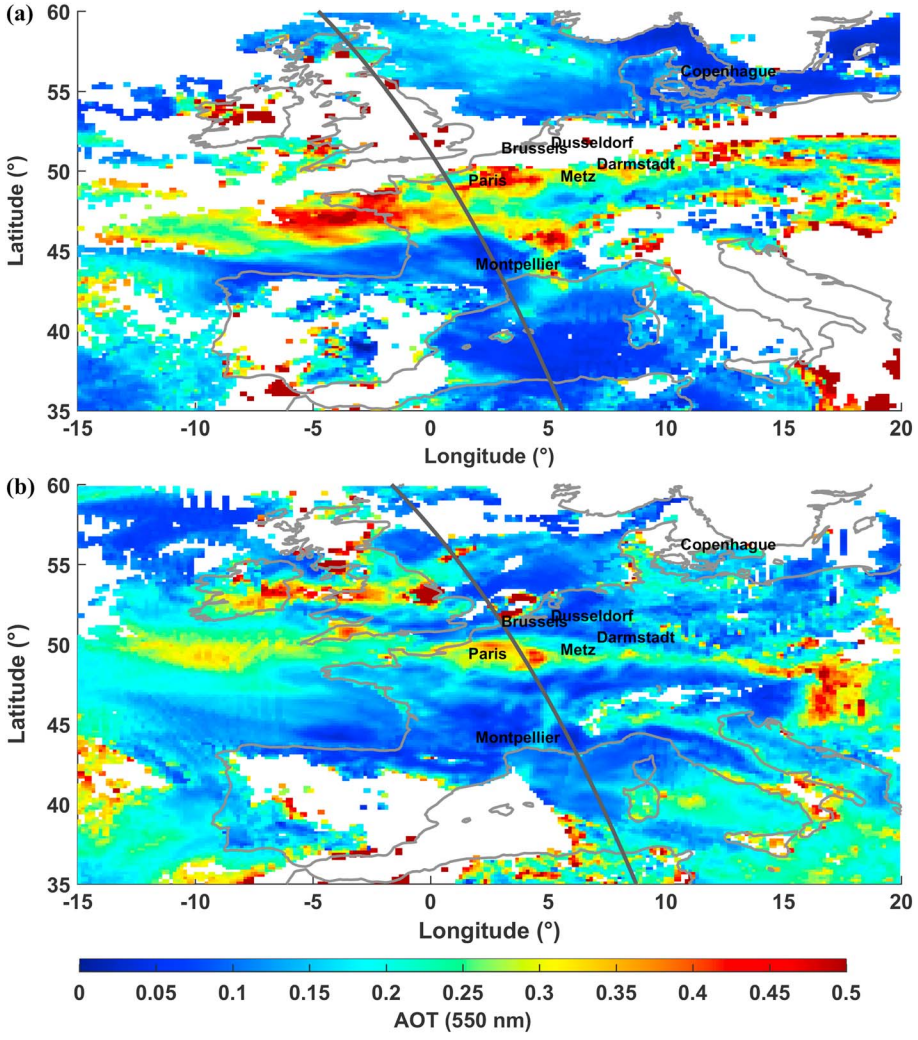

Figure 5. MODIS-Terra and Aqua aerosol optical depth at 550 nm as observed on (a) 5 March 2011 and (b) 23 March 2011. The CALIOP ground tracks are shown by the solid gray lines.

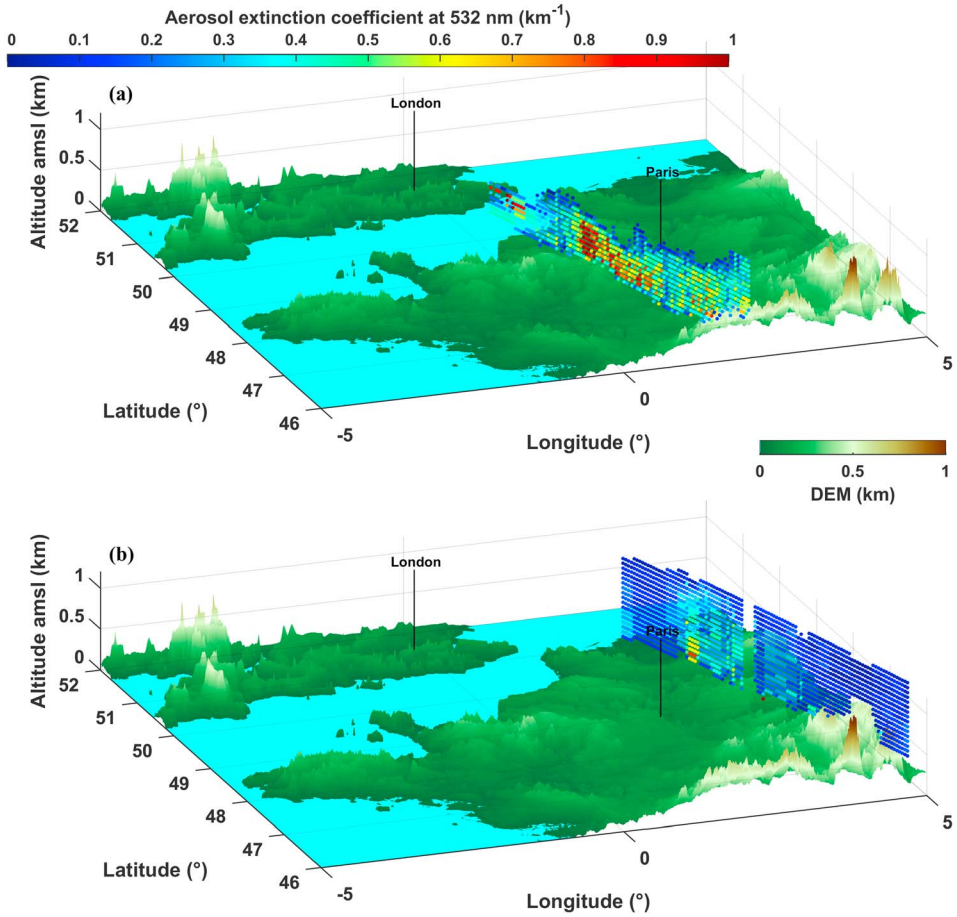

Figure 6. CALIOP-derived aerosol extinction coefficient at 532 nm, as observed on (a) 5 March 2011 and (b) 23 March 2011. DEM is the digital elevation model.

BER, which requires knowing both the scattering phase function and the single-scattering albedo. Note that the Sun photometer-derived single-scattering albedo is not available for level 2 AERONET data after 5 July.

3.2.2. Spaceborne Measurements: A Synoptic View

Satellite measurements from MODIS radiometers and the CALIOP lidar are analyzed to study the spatial extent of the pollution plume over Europe. The results are shown for 5 March in Figures 5a, 6a, and 7a. High AOT at 550 nm (0.3–0.5) are observed in MODIS measurements over the North of France and the Atlantic Ocean (Figure 5a). The pollution plume is extending along the wind direction (from east to west). The pollution plume is also clearly visible on CALIOP-derived EAC at 532 nm between latitudes 45°N and 50°N, with values higher than 0.5 km^{-1}. Mainly, all the pollution is confined to the PBL below 700 m above ground level. CALIOP-derived aerosol classification is shown in Figure 7a. It mainly corresponds with polluted continental aerosols and, to a lesser extent, with polluted dust aerosols in the operational algorithm version 4.10. They correspond with BERs of 0.014 ± 0.005 sr^{-1} (LR = 70 ± 25 sr) and 0.018 ± 0.007 sr^{-1} (LR = 55 ± 22 sr), respectively, matching our findings derived from Sun photometer and our own CALIOP data inversion (Table 2).

Similar comparisons is performed on 23 March 2011, when considering Figure 5b, 6b, and 7b. Both polluted continental and polluted dust aerosols are retrieved along the CALIOP ground track, but with a small additional contribution of dust (BER = 0.025 ± 0.013 sr^{-1} or LR = 40 ± 20 sr) and smoke (BER = 0.014 ± 0.006 sr^{-1} or LR = 70 ± 28 sr). The match with values given in Table 2 is lesser than on 5 March. For the other dates, few lidar profiles can be inversed due to cloud cover.

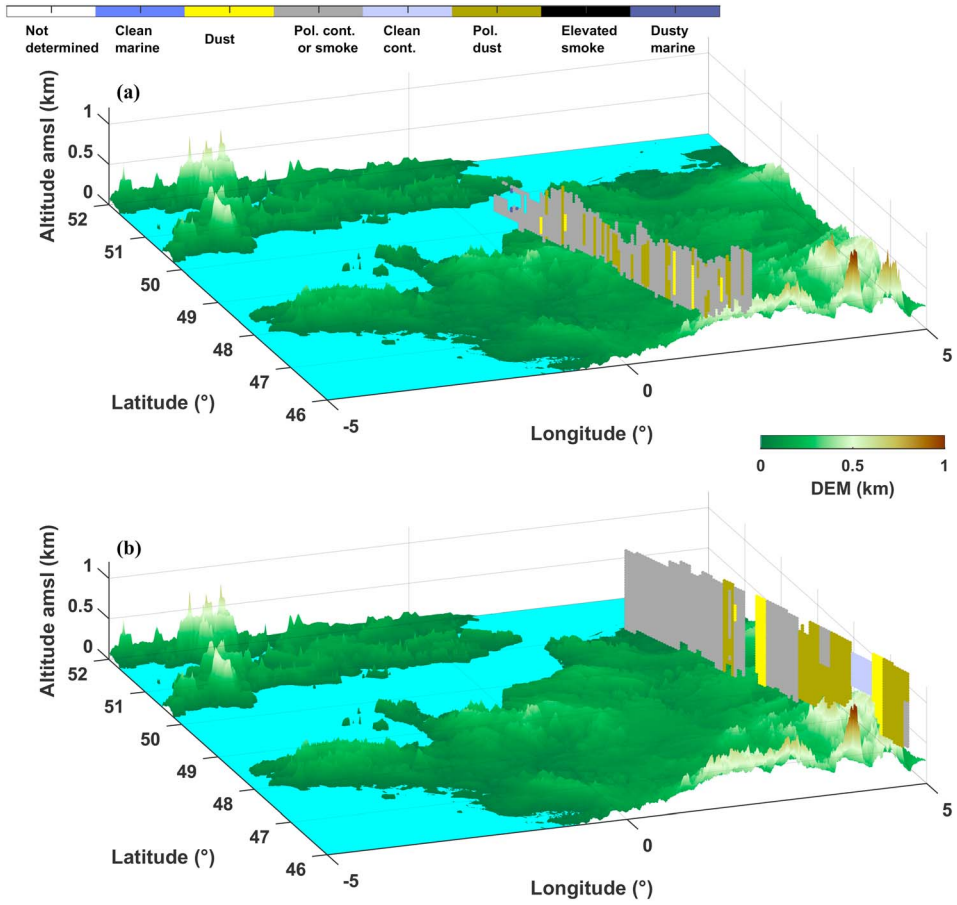

Figure 7. CALIOP-derived aerosol typing (e.g., Polluted continental (Pol. Cont.), clean continental (Clean cont.), or polluted dust (Pol. dust)), as observed on (a) 5 March 2011 and (b) 23 March 2011. DEM is the digital elevation model.

3.3. Meteorological Conditions

During the first case study, a stationary cold anticyclone is positioned above the British Islands on the 3–6 March, which then moves toward Poland on 7 March. This anticyclone is blocking the eastward progression of Atlantic disturbances. It is also associated with two depressions in southwestern Spain and Italy. The meteorological situation during the second pollution event is associated with a large anticyclone located between northern France and the British Islands, which persists between 21 and 23 March. It separates into two lesser anticyclones beginning 24 March, with the first centered over the British Islands and the second one on southern France and Italy. Such circulation field favors the input of pollutants from the east, which is confirmed hereafter by back trajectories. In low wind conditions (1–4 m s^{-1}), it also promotes the accumulation of aerosol pollutants [e.g., *Vautard et al*., 2000].

3.4. Air Mass Origins

For retrieving the air mass origins, back trajectories are computed in ensemble mode using the HYSPLIT model. HYSPLIT is run with 3-hourly archived meteorological data provided by the U.S. National Center for Environmental Prediction Global Data Assimilation System (GDAS) at a horizontal resolution of 0.5°. From Figure 2, the starting altitude is chosen to be 700 m amsl during the two pollution events. Hence, the back trajectories are computed between 3 and 5, and 23 and 25 March 2011 with a time step of 6 h; they are shown in Figures 8a and 8b, respectively.

The pollution aerosols originate from the main polluted areas of Western Europe: Benelux (including Brussels, Belgium, Netherlands, and Luxembourg), Rhine-Ruhr area (including Düsseldorf and Darmstadt, Germany), and the Lorraine area (including Metz, France). The aerosol plume reaches Paris

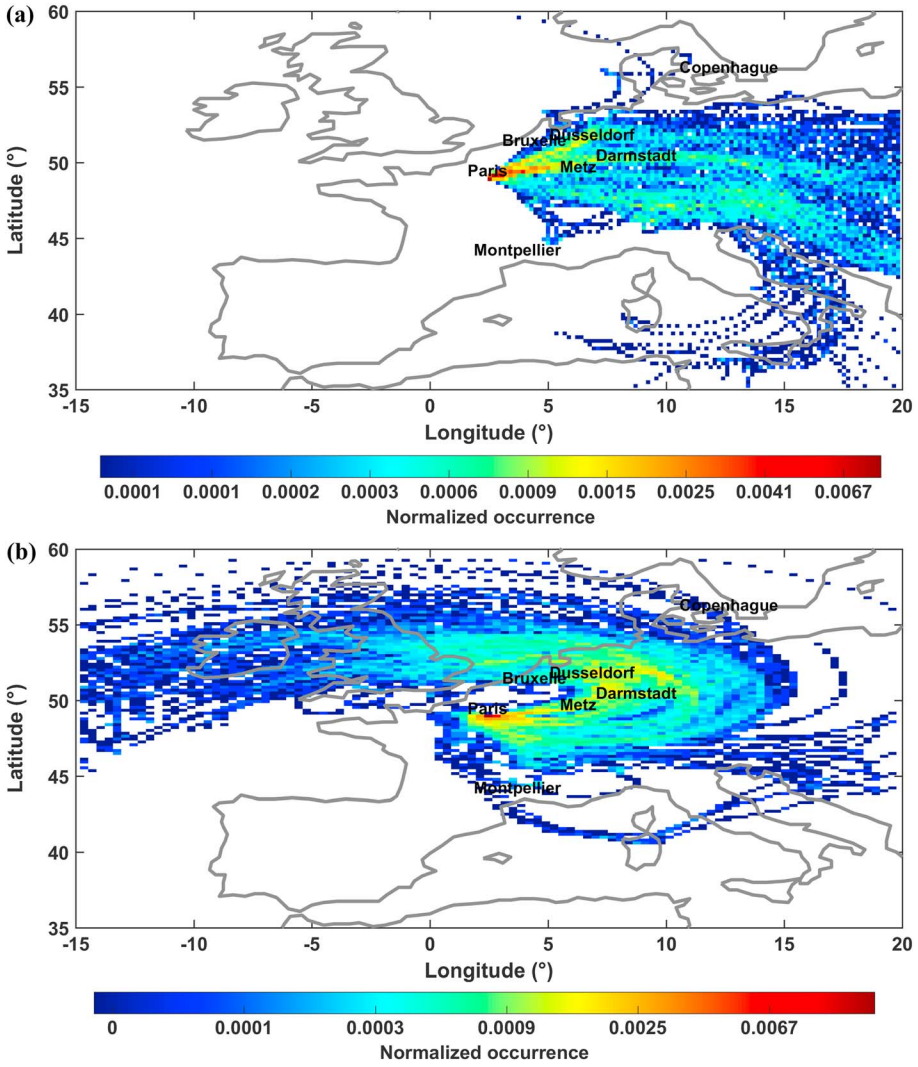

Figure 8. Normalized occurrence of the contribution to the air masses going over the Paris Area from (a) 3 to 5 March 2011 and (b) 23 to 25 March 2011 with a time step of 6 h. The calculations have been done using 3 day back trajectories starting at 700 m amsl with the HYSPLIT model (courtesy of NOAA Air Resources Laboratory; http://www.arl.noaa.gov) in ensemble mode.

after 1 day of transport into the lower troposphere. For the first period (3–5 March), a smaller contribution may be due to the Athens area (not shown), while for the second period (23–25 March), some pollutants may be due to emissions from the United Kingdom. Aerosol origins in the Paris Area have already been studied using positive matrix factorization approach on aerosol chemical components [*Bressi et al.*, 2014]. The transboundary nature of $PM_{2.5}$ pollution at ground level, which is the main contribution to the optical parameters in the Paris Area [*Randriamiarisoa et al.*, 2006], is also shown to be from the same origins.

Secondary semivolatile inorganic aerosols also contribute. Ammonia is emitted by agricultural activities (e.g., animal waste and synthetic fertilizers) along the air mass trajectories. With the low temperatures often encountered during spring pollution episodes associated with anticyclones, agricultural ammonia reacts with the nitric acid from nitrous oxides to form ammonium nitrate aerosols [e.g., *Petetin et al.*, 2016] between northern France and the Paris Area.

The temporal evolutions of the wind lidar-derived horizontal wind speed and direction are shown in Figure 9. The wind speed in the PBL is variable during the first pollution event of the 3–5 March. It ranges between 8 and 17 m s^{-1} before 4 March 1200 LT (local time) and sharply decreases to reach values less than 2 m s^{-1}

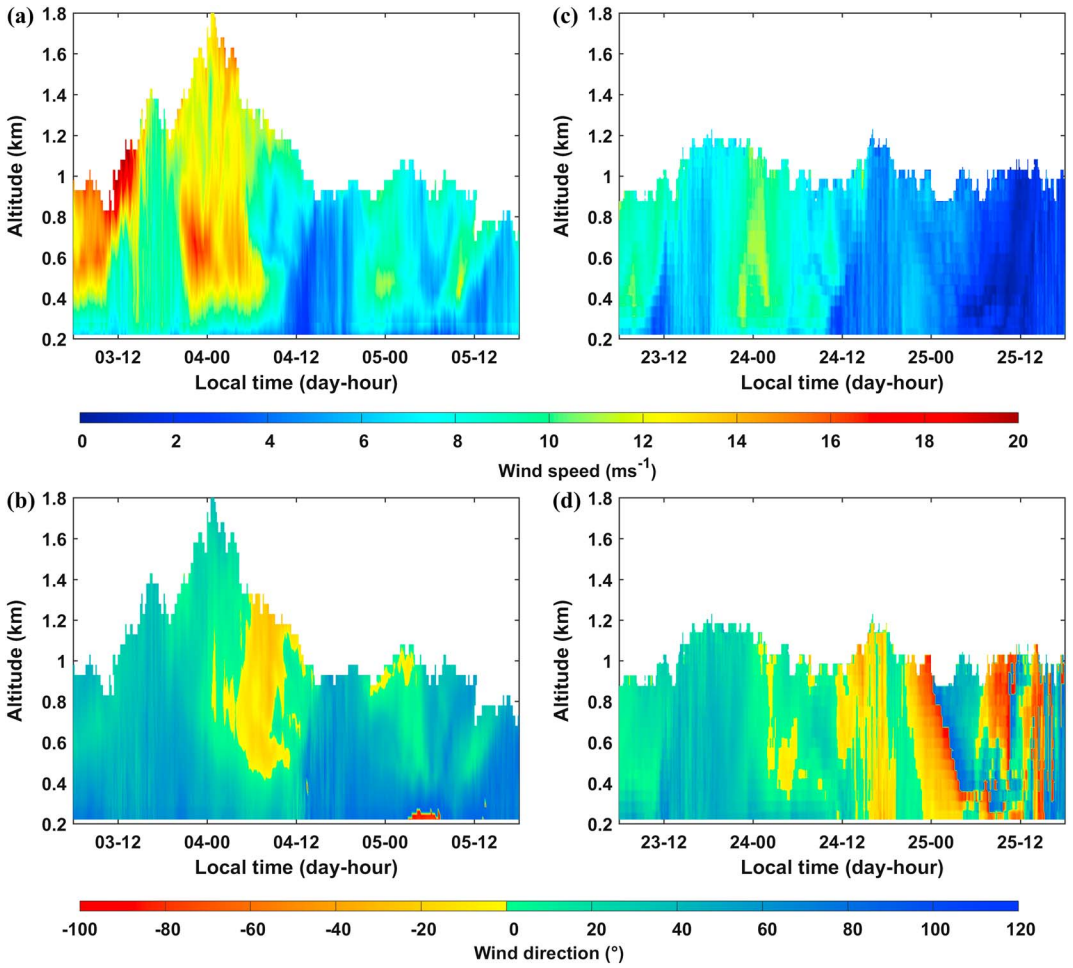

Figure 9. Wind speed and direction from the (a and b) 3 to 5 March 2011 (respectively) and (c and d) the 23 to 25 March 2011 (respectively).

during the second half of the period, thus favoring the local accumulation of particulate pollutants [e.g., *Vautard et al.*, 2000]. The wind direction is mostly northerly and northeasterly, confirming the back trajectories analysis. An important exception is on the morning of 4 March, when the wind direction is rather north-northwest. This evolution is not seen on the temporal evolution of back trajectories shown in Figure 8a. It is therefore certainly linked to a very localized wind shear phenomenon, which does not seem to have a major impact on the aerosol content in the PBL (Figure 2a). For the second pollution event 23–25 March, the wind speed is lower. It does not exceed 12 m s^{-1}, with values close to 1 m s^{-1} for most of that period. These conditions favor air mass stagnation over the Paris Area. The wind direction is variable at low speed and may not be representative. Higher wind speeds are associated with trajectories from the north-northeast.

4. Multiannual Analysis

The good collocation between ground and satellite data for the period of 2011 allows us to consider the joint use of CALIOP and MODIS to analyze the major spring pollution events of the surrounding years. The next step is to analyze whether similar pollution situations to that highlighted for spring 2011 occurred in March and April during the previous and subsequent years or not, and how they can be compared. In what follows, situations where thresholds were exceeded between 2007 and 2016 will be identified and discussed.

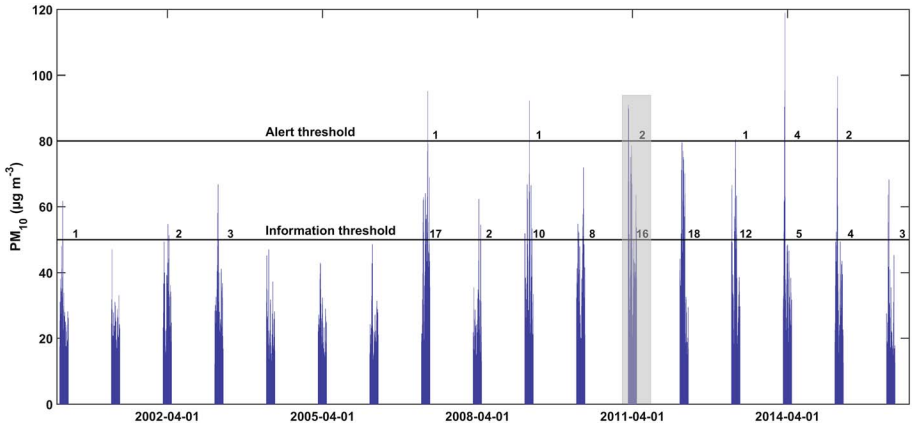

Figure 10. Temporal evolution of mean daily PM_{10} calculated without the input from traffic stations. The thresholds of information and alert are plotted. The number of exceedances is also indicated for both thresholds. The case study of March 2011 is indicated by the shaded area. Only the months of March and April are considered.

4.1. Identification of Aerosol Pollution Event Between 2007 and 2016

The occurrence of pollution events is analyzed using long-term time series data of PM_{10} concentrations, between 2000 and 2016, from the Paris air quality network (AIRPARIF). Figure 10 shows the temporal evolution of mean daily PM_{10}, considering only the months of March and April for each year. Spring 2011 is among the most polluted, with 2 exceedances of the alert threshold and 16 of the information threshold. Four exceedances of the alert threshold are reported on 11–14 March 2014 under an east-west flux (well highlighted on the MODIS AOT products, not shown). There was less pollution occurrence before 2007.

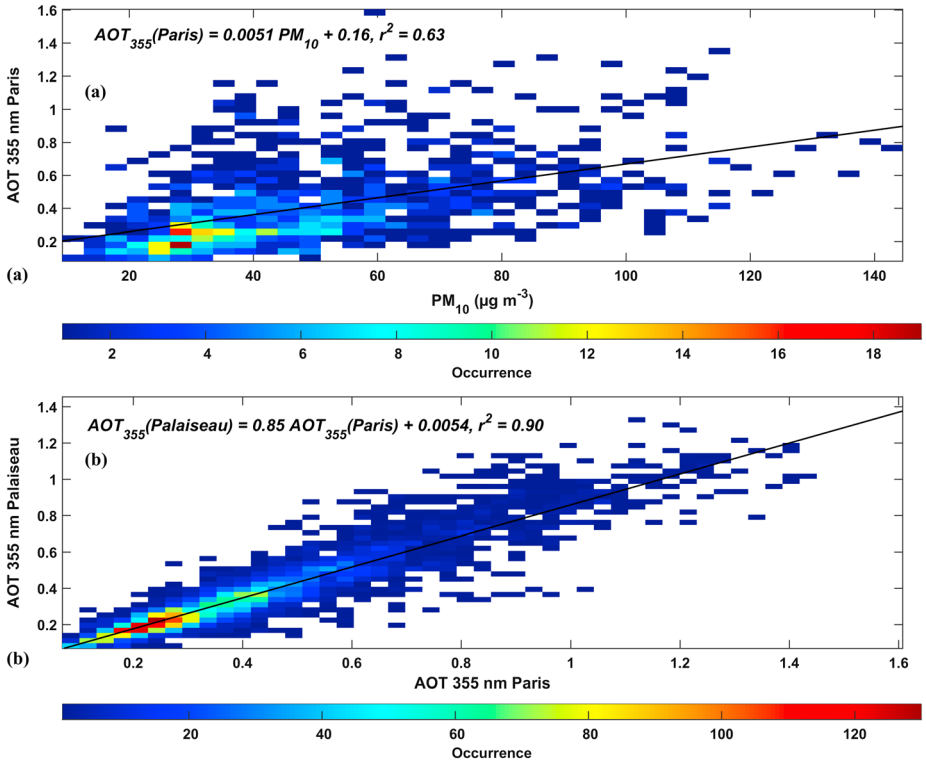

Figure 11. Two-dimensions histogram of (a) the mean daily Sun photometer-derived AOT at 355 nm against the mean daily PM_{10} and (b) the mean daily Sun photometer-derived AOT at 355 nm of Paris and Palaiseau. The input from traffic stations are not considered. The linear fit is drawn in a solid black line; its equation is given. Only the months of March and April are considered.

Table 3. Days of March–April Where the Daily Average PM_{10} Exceeded 80 μg m^{-3} Between 2007 and 2016

Case	Date
1	15 April 2007
2	3 April 2009
3	2 March 2011
4	5 March 2011
5	30 March 2013
6	11 March 2014
7	12 March 2014
8	13 March 2014
9	14 March 2014
10	18 March 2015
11	20 March 2015

The number of available measurement stations has changed from 2006 to 2007, with an increase of one peri-urban station, three urban stations, and one rural station (the traffic stations are not considered). The measurement approach also changed to limit the evaporation of aerosol volatile components (e.g., ammonium nitrate aerosols). This is likely to add a bias (~30%) in the temporal evolution between 2006 and 2007. Hence, the years before 2007 will not be hereafter considered.

4.2. Link Between AOT and PM_{10}

It is also interesting to evaluate whether or not the particulate pollution recorded close to the surface, via PM_{10}, is systematically correlated with the aerosol content in the atmospheric column, as it seems to be for the previous case study. A two-dimensional histogram of the mean daily Sun photometer-derived AOT at 355 nm against the mean daily PM_{10} is given in Figure 11a, for the months of March and April from 2000 to 2016. A correlation exists with r^2 ~ 0.63 for a straight-line equation AOT_{355}(Paris) ~ 0.005 PM_{10} + 0.16, but with strong dispersion around the mean value and a very high bias. This indicates that the measurements of AOT and the lidar are not always good indicators of the instantaneous ground level pollution. Note that *Toth et al.* [2014] have highlighted inconsistencies in surface $PM_{2.5}$ versus satellite-derived AOT. An explanation may be linked to the hygroscopic ammonium nitrate aerosols, which lead to increase the AEC as shown by *Randriamiarisoa et al.* [2006] for water soluble aerosols and more recently by *Morgan et al.* [2010] when they studied the aerosol direct radiative effect, and indirectly by *Kamilli et al.* [2014] when they assessed aerosol hygroscopic growth factors against the aerosol chemical composition. AOT and PM_{10} are nonetheless useful indicators to bring strong constraints to forecasting models [e.g., *Tombette et al.*, 2008; *Wang et al.*, 2013]. The previous calculation was performed for the AERONET station in Paris.

Comparisons between the AERONET stations of Paris and Palaiseau are given in Figure 11b, which represents the two-dimensional histogram of mean daily Sun photometer-derived AOT at 355 nm. The correlation is very good with r^2 ~ 0.90 and a straight-line equation AOT_{355}(Palaiseau) ~ 0.85 AOT_{355}(Paris) + 0.005. Therefore, we find similar conclusions with respect to PM_{10} from the AERONET station of Palaiseau. We note that the AOT is on average 15% lower on Palaiseau, which is not directly influenced by Paris' pollution.

4.3. Link With Meteorological Parameters

Air mass origins are similar during the 11 strong spring pollution cases (daily average $PM_{10} > 80$ μg m^{-3}, Table 3) identified between 2007 and 2016 in Figure 10, as demonstrated using back trajectories calculated at the pressure level of 950 hPa (Figure 12). Scatterplots of maximum daily PM_{10} concentrations versus specific atmospheric parameters (surface pressure, PBL height, wind speed, and wind direction at 950 hPa) extracted from European Centre for Medium-Range Weather Forecasts (ECMWF) Re-Analysis (ERA) at 1200 UTC are shown in Figure 13. The main pollution events are highlighted in blue and red dots, when exceeding the information and alert threshold, respectively. The PM_{10} concentrations are relatively high when ground level pressure increases (Figure 13a), except for

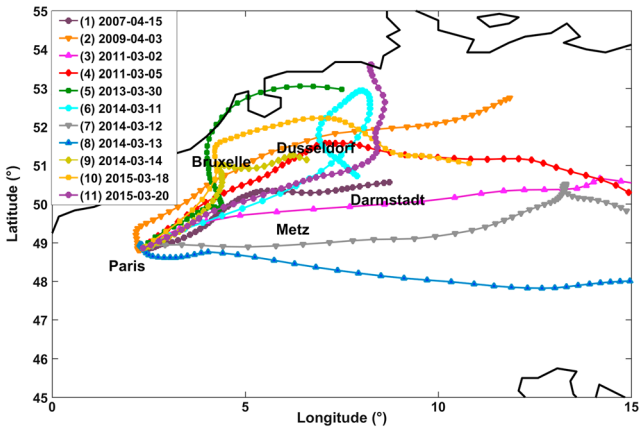

Figure 12. Two days mean back trajectories for the 11 major pollution events ($PM_{10} > 80$ μg m^{-3}) occurring in March–April between 2007 and 2016.

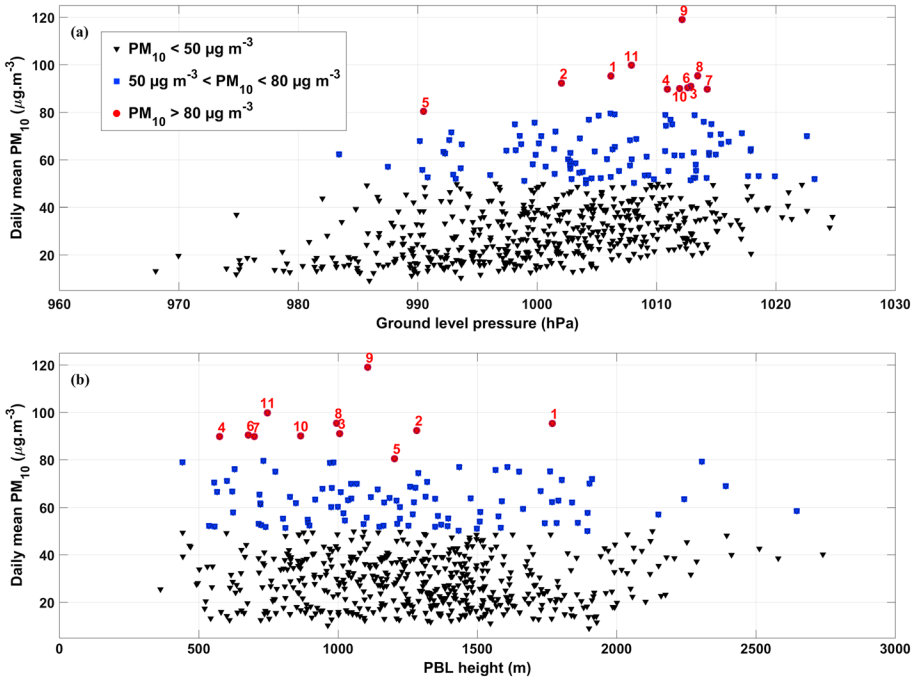

Figure 13. Scatterplots between the maximum daily mean PM_{10} concentrations and (a) the ground level pressure, and (b) the PBL height. The data are given at 1200 UTC for the months of March and April from 2007 to 2016. The pollution events that exceed the information and alert thresholds are represented in blue and red dots, respectively. The alert threshold events are numbered in red.

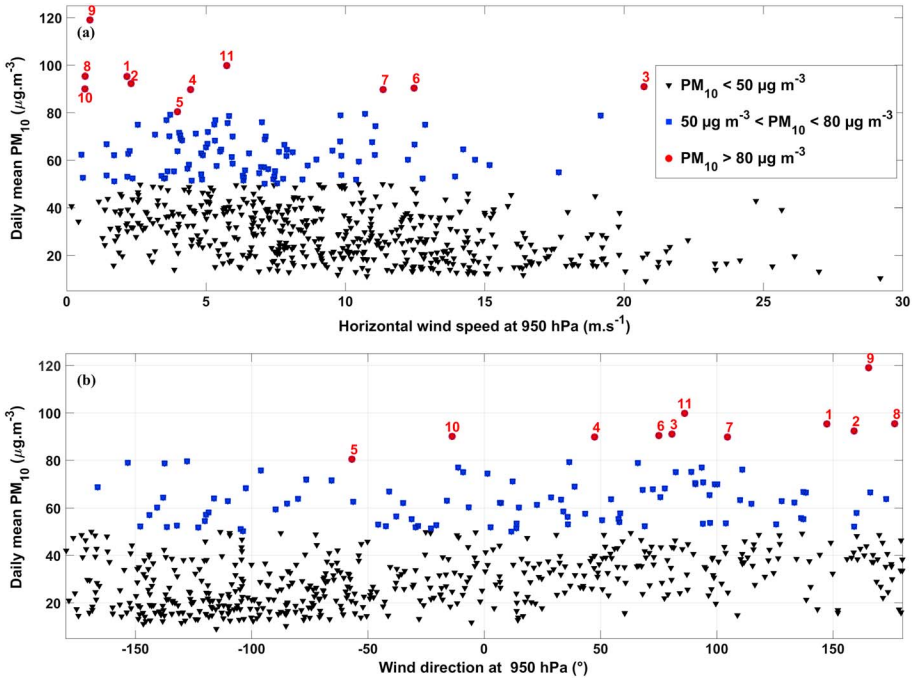

Figure 14. Scatterplots between the maximum daily mean PM_{10} concentrations and (a) the wind speed, and (b) the wind direction at 950 hPa. The data are given at 1200 UTC for the months of March and April from 2007 to 2016. The pollution events that exceed the information and alert thresholds are represented in blue and red dots, respectively. The alert threshold events are numbered in red.

Table 4. Aerosol Optical Properties Found During the 11 Highest Pollution Events Between 2007 and 2016[a]

	CALIOP	Sun Photometer Paris and Palaiseau			MODIS
Case	Obit ***Aerosol typing*** **BER** (sr^{-1})	BER (sr^{-1}) at 532 nm (*N*)	Ångström exponent 440–675 nm	AOT at 550 nm	AOT at 550 nm
1	No overpass	(*6*) 0.015 ± 0.001	1.52 ± 0.11	0.55 ± 0.1	0.53 ± 0.07
2	2009-04-03T02-21-51ZN ***Polluted continental*** **0.014 ± 0.005 (LR = 70 ± 25 sr)**	-	0.80 ± 0.03	1.23 ± 0.08	1.35 ± 0.07
3	2011-03-02T11-51-07ZD ***Polluted dust*** **0.018 ± 0.007 (LR = 55 ± 22 sr)**	-	1.31 ± 0.08	0.31 ± 0.05	0.35 ± 0.02
4	2011-03-05T12-22-22ZD ***Polluted continental*** **0.014 ± 0.005**	(*4*) 0.015 ± 0.001	1.30 ± 0.06	0.53 ± 0.05	0.39 ± 0.04
5	*2013-03-30T12-01-15ZD* ***Polluted continental and polluted dust*** **0.014 ± 0.005 and 0.018 ± 0.007**	-	1.31 ± 0.08	0.31 ± 0.05	-
6	2014-03-11T12-35-51ZD ***Polluted continental and polluted dust*** **0.014 ± 0.005 and 0.018 ± 0.007**	-	0.96 ± 0.06	0.35 ± 0.03	0.35 ± 0.02
7	No overpass	-	1.36 ± 0.05	0.23 ± 0.04	0.24 ± 0.01
8	2014-03-13T12-23-47ZD ***Polluted continental*** **0.014 ± 0.005**	(*3*) 0.013 ± 0.001	1.34 ± 0.04	0.36 ± 0.07	0.42 ± 0.05
9	2014-03-14T02-27-24ZN ***Polluted continental*** **0.014 ± 0.005**	(*6*) 0.014 ± 0.001	1.19 ± 0.05	0.47 ± 0.05	0.44 ± 0.07
10	2015-03-18T12-12-32ZD ***Polluted continental and polluted dust*** **0.014 ± 0.005 and 0.018 ± 0.007**	-	1.06 ± 0.11	0.61 ± 0.09	0.79 ± 0.14
11	2015-03-20T12-00-23ZD ***Polluted continental*** **0.014 ± 0.005**	-	0.97 ± 0.06	0.64 ± 0.02	0.76 ± 0.11

[a]Optical properties are derived from ground-based Sun photometer and the spaceborne instruments MODIS and CALIOP. Aerosol optical thickness (AOT) is given for each passive remote sensing instrument. Backscatter to extinction ratio (BER) and the aerosol typing (in bold italic) are derived from the CALIOP operational products version 4.10 (the lidar ratio (LR) is also given in bold for the main aerosol typing encountered). Number of data *N* is also given for Sun photometer-derived BER. The cases are the ones from Table 3. Cloudy days are highlighted by a gray area.

case 5, on 30 March 2013 with a corresponding ground level pressure of 990 hPa. The PBL height (Figure 13b) is more toward the lower values when strong particulate pollution occurred. Case 1 is rather isolated and associated with a high PBL height (> 1700 m).

Both wind speed and direction are given in Figure 14 at 950 hPa. Most intense pollution events correspond with weak winds (Figure 14a), except for cases 3, 6, and 7. Such meteorological conditions favor air mass stagnation and thus the local enhancement of the aerosol concentration. There is no specific signature in terms of wind direction (Figure 14b) when the wind speed is rather low (< 5 m s^{-1}), and the air masses recirculate over the Paris Area, explaining why the local wind direction does not correspond with the mean air mass back trajectories (Figure 12). Cases 6 to 9 correspond with consecutive days of the same high pollution event in March 2014. The wind speed at 950 hPa was significantly higher during the first 2 days and reached less than 1 m s^{-1} on the 13–14 March 2014. Among all the cases, the highest value (~120 μg m^{-3}) of the daily average PM_{10} is reached on 14 March 2014.

4.4. Coherence With MODIS and CALIOP

In section 3, MODIS and CALIOP data helped characterize major aerosol pollution events. An important finding was the good coherence between the GBL and CALIOP, which allows us to use it with confidence.

For the 11 pollution events listed in Table 3, we seek to identify aerosol typing and evaluate the associated AOTs. The simplest tool is the Sun photometer, and we have reported the daily mean AOTs in Table 4 for

each pollution event. AOTs are quite variable but generally higher or near 0.4 at 550 nm. In case 2 on 3 April 2009, the high value is probably due to a cloud contamination that is not taken into account for MODIS, as it is the Sun photometers. The AOTs deduced from MODIS around Paris (48.65–49.25°N, 2.10–2.55°E) are a very good match with those from the Sun photometer, which reinforces the previous results. What will be noted is that the Ångström exponents are all under 1.5, demonstrating a probable contribution, more or less important, of mineral dusts. A warm meteorological situation facilitates resuspension of particles due to dry soil, and mineral dusts are also present among these aerosols.

For some of the cases, it is possible to extract the BER values from the photometric measurements. They do not significantly change (~ 0.015 sr^{-1}) and are characteristic of what had already been observed over Paris Area, for example, from airborne measurements during the ESQUIF program [*Chazette et al*., 2005]. They are relatively representative of submicron pollution particles. It should be noted that the cases in which the BER could be extracted are associated with the most important values of the Ångström exponents and correspond to cloud-free days.

When available and cloud free, the CALIOP orbits near Paris are used to identify the aerosol pollution plume and deduce aerosol typing via the operational algorithm version 4.10. The results are reported in Table 4. The main typing is polluted continental, which supports our previous conclusions. For some cases, polluted dust typing is also identified within the aerosol plume, which advocates the possible presence of terrigenous particles. The BERs derived from CALIOP are generally between 0.014 and 0.018 sr^{-1}, in reasonable agreement with those derived from the Sun photometers.

5. Conclusion

Based on the synergy between the GBL observations, the measurements of the AIRPARIF air quality monitoring network, and MODIS and CALIPSO spatial observations, two important pollution events of March 2011 occurring in the vicinity of Paris were analyzed. The case study of spring 2011 appears to be one of the most polluted periods in the last decade, with 2 exceedances of the alert threshold and 16 exceedances of the information threshold. A very good match is shown between the optical properties derived from a GBL, Sun photometer, and the spaceborne instruments MODIS and CALIPSO, especially on the identification of aerosol typing. The match also exists when comparing with the inversion of the CALIOP level 1.5 products. The MODIS AOT product emphasizes well the aerosol plume east-west signature and the MODIS-derived AOTs match very well the other available optical measurements. A back trajectory study, initialized by aerosol layers highlighted on the lidar profiles, shows that the pollution aerosols are from the main industrial polluted areas of western Europe: Benelux, Rhine-Ruhr area, and the Lorraine area.

Starting from the case study of spring 2011, we show that the synergy between ground-based and spaceborne observations allows for increasing confidence level for the use of spatial observations, like CALIOP, in order to generalize our analyses over time and space. Hence, a multiannual analysis, from 2007 to 2016, was conducted and showed that similar aerosol typing was present during the 11 major aerosol pollution events identified from the PM_{10} measurements of the AIRPARIF network, with backscatter to extinction ratio between 0.014 and 0.018 sr^{-1} (lidar ratio between 55 and 70 sr). We also showed that the meteorological conditions leading to spring particulate pollution events are quite similar, even when the wind speed stays very low (< 5 ms^{-1}). We note that, even if the AOT and PM_{10} increase in the same direction in both the urban and peri-urban areas, there is no strong correlation between these two variables or at least one with much bias. This can be explained by a significant aerosol transport at altitude above the surface layer and even above the PBL. Our study also suggests that much of the aerosols in all the major pollution events are largely from regional origin (long-range transport) and that the urban increment in Paris is around 15%.

This work stems from a case study whose results are then generalized between 2007 and 2016. We show that there has been no significant change in the aerosol nature since 2007 during the different aerosol major spring pollutions. It is worth noting that we find no significant increase in long-distance pollution over time. Decadal studies are usually conducted from regional modeling. What we show here is that they are also possible, based on an adapted measurement synergy between ground-based and spaceborne remote sensing observations. The long duration of spaceborne missions, such as Terra/Aqua and CALIPSO, is a fundamental asset for monitoring particulate pollution on the scale of large urbanized areas. The idea would be to

generalize this type of approach not only by maintaining the continuity of spatial observations but also by developing measurement networks on ground level equipped with lidar systems which are fundamental for the validation of remote sensing observation from space. Ground-based lidars also introduce new constraints that may significantly improve the predictive capabilities of transport chemistry models via assimilation approaches [e.g., *Wang et al*., 2013, 2014].

Acknowledgments
The authors would like to thank the AIRPARIF network for collecting data. The AIRPARIF data are available at http://www.airparif.asso.fr/en/telechargement/telechargement-station. They also thank the AERONET network for Sun photometer products available at https://aeronet.gsfc.nasa.gov/. The authors acknowledge the MODIS Science team for the Science Algorithms, the Processing Team for producing MODIS data, and the GES DAAC MODIS Data Support Team for making MODIS data available to the user community at https://modis.gsfc.nasa.gov/data/dataprod/. The data processing and distribution of CALIPSO products by the NASA Langley Research Center Atmospheric Sciences Data Center are gratefully acknowledged. The CALIOP level 4.10 data are available at https://eosweb.larc.nasa.gov/HORDERBIN/HTML_Start.cgi. The meteorological data are available at http://climserv.ipsl.polytechnique.fr/fr/les-donnees/ecmwf-analysis-over-global-area-4.html for the ECMWF archive and at http://ready.arl.noaa.gov/archives.php for the GDAS half-degree archive. The ground-based lidar data are available at https://files.lsce.ipsl.fr/public.php?service=files&t=b401396461cb6bd8011d4bb774ec8551. This work was supported by the Commissariat à l'Energie Atomique et aux énergies alternatives (CEA). The Centre National d'Etude Spatial (CNES) helped to maintain the lidar instrument.

References

Amann, M., I. Bertok, R. Cabala, J. Cofala, C. Heyes, F. Gyarfas, Z. Klimont, W. Schöpp, and F. Wagner (2005), A final set of scenarios for the Clean Air for Europe (CAFE) programme, CAFE Scenario Anal. Rep. No. 6, Int. Inst. for Appl. Anal., Laxenburg, Seiten.

Beekmann, M., et al. (2015), In situ, satellite measurement and model evidence on the dominant regional contribution to fine particulate matter levels in the Paris megacity, *Atmos. Chem. Phys.*, *15*(16), 9577–9591, doi:10.5194/acp-15-9577-2015.

Berthier, S., P. Chazette, P. Couvert, J. Pelon, F. Dulac, F. Thieuleux, C. Moulin, and T. Pain (2006), Desert dust aerosol columnar properties over ocean and continental Africa from Lidar in-Space Technology Experiment (LITE) and Meteosat synergy, *J. Geophys. Res.*, *111*, D21202, doi:10.1029/2005JD006999.

Bressi, M., et al. (2014), Sources and geographical origins of fine aerosols in Paris (France), *Atmos. Chem. Phys.*, *14*(16), 8813–8839, doi:10.5194/acp-14-8813-2014.

Brook, R. D., et al. (2004), Air pollution and cardiovascular disease: A statement for healthcare professionals from the expert panel on population and prevention science of the American Heart Association, *Circulation*, *109*(21), 2655–2671, doi:10.1161/01.CIR.0000128587.30041.C8.

Burton, S. P., et al. (2015), Observations of the spectral dependence of linear particle depolarization ratio of aerosols using NASA Langley airborne high spectral resolution lidar, *Atmos. Chem. Phys.*, *15*(23), 13,453–13,473, doi:10.5194/acp-15-13453-2015.

Chauhan, A. J., and S. L. Johnston (2003), Air pollution and infection in respiratory illness, *Br. Med. Bull.*, *68*, 95–112, doi:10.1093/bmb/ldg022.

Chazette, P., H. Randriamiarisoa, J. Sanak, P. Couvert, and C. Flamant (2005), Optical properties of urban aerosol from airborne and ground-based in situ measurements performed during the Etude et Simulation de la Qualité de l'air en Ile de France (ESQUIF) program, *J. Geophys. Res.*, *110*, D02206, doi:10.1029/2004JD004810.

Chazette, P., A. Dabas, J. Sanak, M. Lardier, and P. Royer (2012), French airborne lidar measurements for Eyjafjallajökull ash plume survey, *Atmos. Chem. Phys.*, *12*(15), 7059–7072, doi:10.5194/acp-12-7059-2012.

Chazette, P., J. Totems, G. Ancellet, J. Pelon, and M. Sicard (2015), Temporal consistency of lidar observables during aerosol transport events in the framework of the ChArMEx/ADRIMED campaign at Menorca Island in June 2013, *Atmos. Chem. Phys. Discuss.*, *15*(22), 32,723–32,757, doi:10.5194/acpd-15-32723-2015.

Chazette, P., J. Totems, G. Ancellet, J. Pelon, and M. Sicard (2016), Temporal consistency of lidar observations during aerosol transport events in the framework of the ChArMEx/ADRIMED campaign at Minorca in June 2013, *Atmos. Chem. Phys.*, *16*(5), 2863–2875, doi:10.5194/acp-16-2863-2016.

Chew, B. N., J. R. Campbell, J. S. Reid, D. M. Giles, E. J. Welton, S. V. Salinas, and S. C. Liew (2011), Tropical cirrus cloud contamination in sun photometer data, *Atmos. Environ.*, *45*(37), 6724–6731, doi:10.1016/j.atmosenv.2011.08.017.

Chu, D. A., Y. J. Kaufman, C. Ichoku, L. A. Remer, D. Tanré, and B. N. Holben (2002), Validation of MODIS aerosol optical depth retrieval over land, *Geophys. Res. Lett.*, *29*(12), 8007, doi:10.1029/2001GL013205.

Draxler, R. R., and G. D. Rolph (2015), *HYSPLIT (HYbrid Single-Particle Lagrangian Integrated Trajectory) Model Access Via NOAA ARL READY Website*, NOAA Air Resour. Lab, Silver Spring, Md.

Finardi, S., C. Silibello, A. D'Allura, and P. Radice (2014), Analysis of pollutants exchange between the Po Valley and the surrounding European region, *Urban Clim.*, *10*, 682–702, doi:10.1016/j.uclim.2014.02.002.

Freutel, F., et al. (2013), Aerosol particle measurements at three stationary sites in the megacity of Paris during summer 2009: Meteorology and air mass origin dominate aerosol particle composition and size distribution, *Atmos. Chem. Phys.*, *13*(2), 933–959, doi:10.5194/acp-13-933-2013.

Gladtke, D. (1998), Air pollution in the Rhine-Ruhr-area, *Toxicol. Lett.*, *96–97*, 277–283, doi:10.1016/S0378-4274(98)00083-6.

Highwood, E. J., et al. (2007), Aerosol Direct Radiative Impact Experiment (ADRIEX) overview, *Society*, *15*, 3–15, doi:10.1002/qj.

Holben, B. N., et al. (1998), AERONET—A federated instrument network and data archive for aerosol characterization, *Remote Sens. Environ.*, *66*(1), 1–16, doi:10.1016/S0034-4257(98)00031-5.

Johnson, B. T., B. Heese, S. A. McFarlane, P. Chazette, A. Jones, and N. Bellouin (2008), Vertical distribution and radiative effects of mineral dust and biomass burning aerosol over West Africa during DABEX, *J. Geophys. Res.*, *113*, D00C12, doi:10.1029/2008JD009848.

Kamilli, K. A., L. Poulain, A. Held, A. Nowak, W. Birmili, and A. Wiedensohler (2014), Hygroscopic properties of the Paris urban aerosol in relation to its chemical composition, *Atmos. Chem. Phys.*, doi:10.5194/acp-14-737-2014.

King, M. D., Y. J. Kaufman, W. P. Menzel, and D. Tanré (1992), Remote sensing of cloud, aerosol, and water vapor properties from the Moderate Resolution Imaging Spectrometer (MODIS), *IEEE Trans. Geosci. Remote Sens.*, *30*(1), 2–27, doi:10.1109/36.124212.

Klett, J. D. J. D. (1985), Lidar inversion with variable backscatter/extinction ratios, *Appl. Opt.*, *24*(11), 1638, doi:10.1364/AO.24.001638.

McMeeking, G. R., et al. (2012), Airborne measurements of trace gases and aerosols over the London metropolitan region, *Atmos. Chem. Phys.*, *12*(11), 5163–5187, doi:10.5194/acp-12-5163-2012.

Morgan, W. T., et al. (2010), Enhancement of the aerosol direct radiative effect by semi-volatile aerosol components: Airborne measurements in north-western Europe, *Atmos. Chem. Phys.*, *10*, 8151–8171, doi:10.5194/acp-10-8151-2010.

Patashnick, H., and E. G. Rupprecht (1991), Continuous PM-10 measurements using the tapered element oscillating microbalance, *J. Air Waste Manage. Assoc.*, *41*(8), 1079–1083, doi:10.1080/10473289.1991.10466903.

Petetin, H., J. Sciare, M. Bressi, V. Gros, A. Rosso, O. Sanchez, R. Sarda-Estève, J.-E. Petit, and M. Beekmann (2016), Assessing the ammonium nitrate formation regime in the Paris megacity and its representation in the CHIMERE model, *Atmos. Chem. Phys.*, *16*(16), 10,419–10,440, doi:10.5194/acp-16-10419-2016.

Pikridas, M., et al. (2015), In situ formation and spatial variability of particle number concentration in a European megacity, *Atmos. Chem. Phys.*, *15*(17), 10,219–10,237, doi:10.5194/acp-15-10219-2015.

Pope, C. A., R. T. Burnett, M. J. Thun, E. E. Calle, D. Krewski, K. Ito, and G. D. Thurston (2002), Lung cancer, cardiopulmonary mortality, and long-term exposure to fine particulate air pollution, *JAMA*, *287*(9), 1132–1141, doi:10.1016/j.scitotenv.2011.03.017.

Pope, C. A., M. Ezzati, D. W. Dockery, C. A. Pope III, M. Ezzati, and D. W. Dockery (2009), Fine-particulate air pollution and life expectancy in the United States, *N. Engl. J. Med.*, *360*(4), 376–386, doi:10.1056/NEJMsa0805646.

Randriamiarisoa, H., P. Chazette, P. Couvert, J. Sanak, and G. Mégie (2006), Relative humidity impact on aerosol parameters in a Paris suburban area, *Atmos. Chem. Phys.*, *6*(5), 1389–1407, doi:10.5194/acp-6-1389-2006.

Raut, J., and P. Chazette (2007), Retrieval of aerosol complex refractive index from a synergy between lidar, sunphotometer and in situ measurements during LISAIR experiment, *Atmos. Chem. Phys.*, *7*(2001), 2797–2815.

Raut, J. C., and P. Chazette (2009), Assessment of vertically-resolved PM10 from mobile lidar observations, *Atmos. Chem. Phys.*, *9*(21), 8617–8638.

Royer, P., J.-C. Raut, G. Ajello, S. Berthier, and P. Chazette (2010), Synergy between CALIOP and MODIS instruments for aerosol monitoring: Application to the Po Valley, *Atmos. Meas. Tech.*, *3*(4), 893–907, doi:10.5194/amt-3-893-2010.

Royer, P., P. Chazette, M. Lardier, and L. Sauvage (2011a), Aerosol content survey by mini N2-Raman lidar: Application to local and long-range transport aerosols, *Atmos. Environ.*, *45*(39), 7487–7495, doi:10.1016/j.atmosenv.2010.11.001.

Royer, P., P. Chazette, K. Sartelet, Q. J. Zhang, M. Beekmann, and J. C. Raut (2011b), Comparison of lidar-derived PM_{10} with regional modeling and ground-based observations in the frame of MEGAPOLI experiment, *Atmos. Chem. Phys.*, *11*(20), 10,705–10,726.

Salomonson, V. V., W. L. Barnes, P. W. Maymon, H. E. Montgomery, and H. Ostrow (1989), MODIS: Advanced facility instrument for studies of the Earth as a system, *IEEE Trans. Geosci. Remote Sens.*, *27*(2), 145–153, doi:10.1109/36.20292.

Stephens, G. L., et al. (2002), The Cloudsat mission and the A-Train: A new dimension of space-based observations of clouds and precipitation, *Bull. Am. Meteorol. Soc.*, *83*(12), 1771–1790, doi:10.1175/BAMS-83-12-1771.

Tombette, M., P. Chazette, B. Sportisse, and Y. Roustan (2008), Simulation of aerosol optical properties over Europe with a 3-D size-resolved aerosol model: Comparisons with AERONET data, *Atmos. Chem. Phys.*, *8*(23), 7115–7132, doi:10.5194/acp-8-7115-2008.

Toth, T. D., J. Zhang, J. R. Campbell, E. J. Hyer, J. S. Reid, Y. Shi, and D. L. Westphal (2014), Impact of data quality and surface-to-column representativeness on the PM 2.5 / satellite AOD relationship for the contiguous United States, *Atmos. Chem. Phys.*, *14*, 6049–6062, doi:10.5194/acp-14-6049-2014.

Vautard, R., et al. (2000), Measurements and modeling of atmospheric pollution over the Paris area: An overview of the ESQUIF project, *Ann. Geophys.*, *18*(11), 1467–1481.

Vautard, R., et al. (2003), A synthesis of the Air Pollution Over the Paris Region (ESQUIF) field campaign, *J. Geophys. Res.*, *108*(D17), 8558, doi:10.1029/2003JD003380.

Wang, Y., K. N. Sartelet, M. Bocquet, and P. Chazette (2013), Assimilation of ground versus lidar observations for PM_{10} forecasting, *Atmos. Chem. Phys.*, *13*(1), 269–283, doi:10.5194/acp-13-269-2013.

Wang, Y., K. N. Sartelet, M. Bocquet, and P. Chazette (2014), Modelling and assimilation of lidar signals over greater Paris during the MEGAPOLI summer campaign, *Atmos. Chem. Phys.*, *14*(7), 3511–3532, doi:10.5194/acp-14-3511-2014.

Winker, D. M., J. Pelon, M. P. Mccormick, U. Pierre, and P. Jussieu (2003), The CALIPSO mission: Spaceborne lidar for observation of aerosols and clouds, *Proc. SPIE*, *4893*, 1–11, doi:10.1117/12.466539.

Winker, D. M., W. H. Hunt, and M. J. McGill (2007), Initial performance assessment of CALIOP, *Geophys. Res. Lett.*, *34*, L19803, doi:10.1029/2007GL030135.